Wu and Gao *Chin. J. Mech. Eng.* (2018) 31:50
https://doi.org/10.1186/s10033-018-0253-2

Chinese Journal of Mechanical Engineering

ORIGINAL ARTICLE

Open Access

Parameter Optimization of a Stability-Training Platform's 4-PSS/PS Parallel Mechanism Based on Training Ability Evaluation Index and PSO Algorithm

Wei-Guo Wu* and Li-Yang Gao

Abstract

The existing mechanism parameter optimization (MPO) method of parallel mechanisms only considers the workspace size and ignores contribution of each configuration's performance. So a novel MPO method is proposed for our serial-parallel mechanism platform, which is used in stability training of legged robots. Regarding the platform's parallel mechanism part, a 4-PSS/PS parallel mechanism, two object functions and three constraint conditions are defined to establish the MPO model. The first object function uses critical motion indexes of the moving platform. The second one uses derivative function of the defined disturbance Lagrange function. After analyzing stability-training requirements of five existing legged robots, requirements of the platform's motion capability are given out. Regarding each proposed object function separately, the MPO model is solved by the particle swarm optimization (PSO) algorithm. Valid workspace boundaries corresponding to the optimization results are solved by a numerical method. The overall optimal solution is determined based on volume of the valid workspace. It is revealed that the two object functions result in similar optimization solutions, which shows that the proposed object functions can reflect the stability-training ability consistently. This paper proposes and verifies the established MPO model, which considers both the workspace size and configurations' performance evaluation.

Keywords: Stability training, 4-PSS/PS parallel mechanism, Mechanism parameter optimization, Singularity analysis, Particle swarm optimization

1 Introduction

Legged robots influenced by the environment disturbance may be unstable, so balancing control is needed to obtain the self-stabilizing ability. Thus, for different environment disturbances, different balancing controllers were designed based on the dynamics model, such as: the balancing controllers for walking on uneven terrain or a slope [1–4], the balancing controllers for standing on a tilting slope [2, 5–7], the balancing controllers against external impacts [2, 5, 8], and so on. These controllers are influenced by the model error. And each controller is only designed for a specific robot motion (standing, walking, etc.) and a specific environment disturbance (tilting ground, impact forces, etc.), which leads to less versatility.

In order to reduce the dependency to the dynamics model, intelligence algorithms were applied to design intelligence stabilizers, such as: the fuzzy algorithm [9, 10], the artificial neural networks [11], the reinforcement learning algorithm [12, 13], and so on. And some stabilizers' versatility were enhanced. Wasielica [14] designed a static stabilizer for arbitrary upper-body motions on a tilting platform. In order to get the best similarity and stability, Vuga et al. [13] modified the reproduced human motion samples by a reinforcement learning stabilizer.

It was hard to cover all kinds of environment disturbances in the design stage of the mentioned controllers. Also, the disturbances applied in the learning stage of the intelligence stabilizers were relatively single. So

*Correspondence: wuwg@hit.edu.cn
School of Mechatronics Engineering, Harbin Institute of Technology, Harbin 150001, China

it is hard to get the self-stabilizing ability with strong robustness, neither can get the animal-like global self-stabilizing ability, which keeps balancing against arbitrary disturbances within the driving ability limitation.

Toward this problem, the authors designed a serial-parallel mechanism platform (Figure 1(a)) with 6 degree-of-freedoms (DOFs) [15, 16], and proposed the idea of obtaining robot's self-stabilizing ability by actively training (Figure 1(b)). During the training process, the training platform applied random motions with limited amplitude to disturb the trained robots. The robots modify their motion based on platform position and orientation feedback, robot joint position feedback and contacting force feedback. The global self-stabilizing ability can be obtained by learning.

Parallel mechanism part of the designed platform is a 4-PSS/PS parallel mechanism, and the serial mechanism part is a 2-DOF translational mechanism fixed on the moving platform. The platform has a low, big-size moving platform with big workspace, high speed and acceleration. So it is convenient for robots to get on or off the moving platform. And the protective equipment can be installed on the moving platform. Compared to the Stewart platform and other newly proposed motion platforms [17–20], the designed platform is more suitable for the stability training. To improve the training performance, MPO of the 4-PSS/PS mechanism will conducted in this paper.

Regarding to the MPO issue, dexterity evaluation indexes were proposed based on the Jacobian matrix of the mechanism's kinematics, such as: the manipulability [21], the condition number [22] and the global condition number [23]. Considering influence of the assembly error and the control error on the position precision of the tip (or the moving platform of parallel mechanisms), Caro et al. [24] defined a sensitivity index based on the norm of the Jacobian matrix. And they compared the sensitivity indexes of several planer mechanisms [25]. Rezaei et al. [26] evaluated the direct sensitivity and the inverse sensitivity of a 3-PSP mechanism by moving platform's max position and orientation error. Based on the Krawczyk operator, Tannous et al. [27] proposed an interval linearization method to speed up the sensitivity-based MPO calculation. The mentioned evaluation indexes are all focused on singularity aspect of a mechanism configuration, rather than the performance contribution of the workspace size.

On the other side, volume of the non-singularity workspace was used to evaluate parallel mechanisms. Based on the Lagrange multiplier method, Li et al. [28] solved the largest non-singular spherical workspace of a 3-RPR mechanism. By the same method, Fu and Gao [29] proposed an approach to minimize mechanism's volume while its workspace is determined. Karimi et al. [30] solved the largest non-singular workspace of the 6-UPS mechanism by the convex optimization algorithm. Kaloorazi et al. [31] solved the largest non-singular circle in workspace of a 3-PRR mechanism by the geometric method. And Hou et al. [32] solved the largest reachable workspace of the 3-PSS/S mechanism by the genetic algorithm. However, these methods treated the whole workspace equally, rather than evaluating each mechanism configuration separately.

For the shortcomings of the existing mechanism evaluation indexes, this paper gives out three constraint conditions of solving the valid workspace: mechanism singularity, active pairs' speed limitation and driving force limitation. And two evaluation indexes of the training ability are proposed for each mechanism configuration. One of them is based on the critical motion index of the moving platform. The other is based on derivative function of the disturbance Lagrange function. By integration in the workspace, MPO object function is proposed for each evaluation index, which considers both workspace's size and the training performance of each mechanism configuration. So compared with the existing evaluation method, the proposed method can evaluate 4-PSS/PS mechanism's training ability more comprehensively.

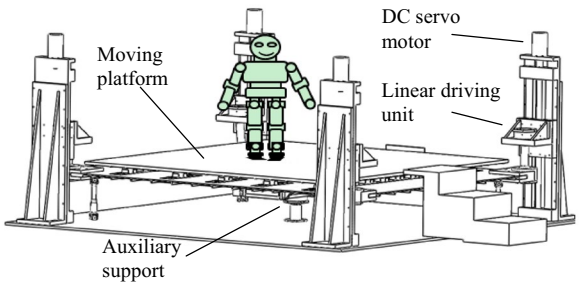

(a) 6 DOF serial-parallel mechanism platform [15]

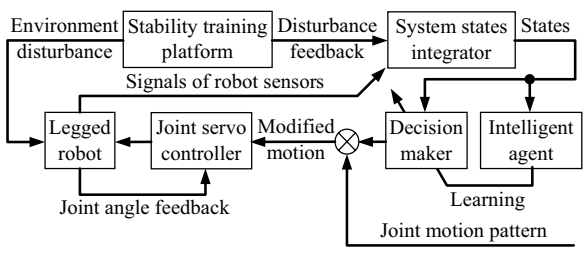

(b) Stability training concept

Figure 1 Stability training platform and the stability training concept

2 4-PSS/PS Mechanism and its Kinematics Equations

The parallel mechanism part of the stability-training platform is a 4-PSS/PS parallel mechanism (shown in Figure 2). The prismatic pairs in four PSS kinematics chains

are active kinematics pairs. A_i and B_i ($i=1, 2, 3, 4$) are centers of upper and lower spherical pairs in the PSS kinematics chains respectively. Distance between A_i and B_i is L_0. C is center of the spherical pair in the PS kinematics chain. The projection of C on the ground is the center of the rectangular formed by the projections of A_i. Also, C is the center of the moving platform. Right-handed coordinate frame ΣO-xyz is the base coordinate frame. Point O is located at the projection of C on the ground. Coordinate frame ΣC-uvw is the moving coordinate frame fixed with the moving platform. Positive directions of the coordinate axes are shown in Figure 2. The mechanism parameter set of the 4-PSS/PS mechanism is $\{L_0, L_1, L_2, L_3, L_4\}$.

The 4-PSS/PS mechanism has 4 DOFs: translation along vertical direction and three posture DOFs. So workspace of this mechanism is considered to be a 4-dimensional space spanned by z, θ_r, θ_p, θ_y, which are position and orientation parameters of the moving platform, respectively representing the height, roll angle, pitch angle, yaw angle of ΣC-uvw in the base coordinate frame. The kinematics equations in vector form can be written as

$$\left\|\boldsymbol{P}_{Ai}-\boldsymbol{T}\left(\theta_r,\theta_p,\theta_y,z\right)\boldsymbol{P'}_{Bi}\right\|-L_0^2=0, \tag{1}$$

where $i=1, 2, 3, 4$ (corresponding to the four PSS kinematics chains); $\boldsymbol{P}_{Ai}$ represents homogeneous position coordinate vectors of A_i in ΣO-xyz; and $\boldsymbol{P'}_{Bi}$ represents homogeneous position coordinate vectors of B_i in ΣC-uvw; $\boldsymbol{T}$ is the homogeneous transformation matrix of ΣC-uvw relative to ΣO-xyz, which is a function of the four position and orientation parameters with the expression

$$\boldsymbol{T}\left(\theta_r,\theta_p,\theta_y,z\right)=\begin{bmatrix} c_pc_r & s_pc_rs_y-c_ys_r & s_pc_rc_y+s_ys_r & 0\\ c_ps_r & s_ps_rs_y+c_ys_r & s_ps_rc_y-s_yc_r & 0\\ -s_p & c_ps_y & c_pc_y & z\\ 0 & 0 & 0 & 1\end{bmatrix}, \tag{2}$$

where $c_j=\cos\theta_j$ and $s_j=\sin\theta_j$ ($j=$ r, p, y).

Based on Eq. (1), the derivative kinematics equation can be deduced as

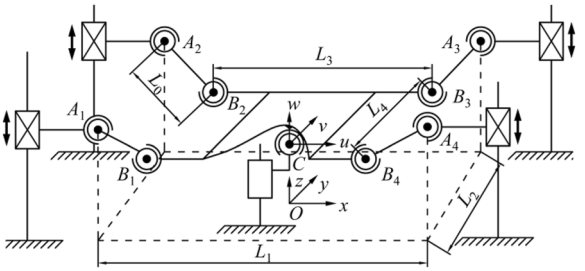

Figure 2 4-PSS/PS mechanism

$$2\left(\boldsymbol{P}_{Ai}-\boldsymbol{T}\boldsymbol{P'}_{Bi}\right)^{\mathrm{T}}\left\{\begin{bmatrix}0 & 0 & \dot{z}_{Ai} & 0\end{bmatrix}^{T}-\dot{\boldsymbol{T}}\boldsymbol{P'}_{Bi}\right\}=0, \tag{3}$$

where $\dot{z}_{Ai}$ is vertical velocity of A_i in the base coordinate frame ($i=1, 2, 3, 4$); $\dot{\boldsymbol{T}}$ is time derivative matrix of the homogeneous transformation matrix.

Eq. (3) can be written in a matrix form as

$$\boldsymbol{A}(\boldsymbol{x})\dot{\boldsymbol{Z}}=\boldsymbol{B}(\boldsymbol{x})\dot{\boldsymbol{x}}, \tag{4}$$

where $\dot{\boldsymbol{Z}}=\begin{bmatrix}\dot{z}_{A1} & \dot{z}_{A2} & \dot{z}_{A3} & \dot{z}_{A4}\end{bmatrix}^{\mathrm{T}}$ is the velocity vector of the active prismatic pairs; $\boldsymbol{x}=[\theta_r, \theta_p, \theta_y, z]^{\mathrm{T}}$ is configuration vector of the moving platform and $\dot{\boldsymbol{x}}$ is its velocity vector. $\boldsymbol{A}(\boldsymbol{x})$ and $\boldsymbol{B}(\boldsymbol{x})$ have following expressions:

$$\boldsymbol{A}(\boldsymbol{x})=\mathrm{diag}\left(\begin{bmatrix}\boldsymbol{e}_3^{\mathrm{T}}\left(\boldsymbol{P}_{A1}-\boldsymbol{T}\boldsymbol{P'}_{B1}\right)\\ \boldsymbol{e}_3^{\mathrm{T}}\left(\boldsymbol{P}_{A2}-\boldsymbol{T}\boldsymbol{P'}_{B2}\right)\\ \boldsymbol{e}_3^{\mathrm{T}}\left(\boldsymbol{P}_{A3}-\boldsymbol{T}\boldsymbol{P'}_{B3}\right)\\ \boldsymbol{e}_3^{\mathrm{T}}\left(\boldsymbol{P}_{A4}-\boldsymbol{T}\boldsymbol{P'}_{B4}\right)\end{bmatrix}\right),$$

$$\boldsymbol{B}(\boldsymbol{x})=\begin{bmatrix}\left(\boldsymbol{P}_{A1}-\boldsymbol{T}\boldsymbol{P'}_{B1}\right)^{\mathrm{T}}\begin{bmatrix}\frac{\partial\boldsymbol{T}}{\partial z} & \frac{\partial\boldsymbol{T}}{\partial\theta_r} & \frac{\partial\boldsymbol{T}}{\partial\theta_p} & \frac{\partial\boldsymbol{T}}{\partial\theta_y}\end{bmatrix}\boldsymbol{P'}_{B1}\\ \left(\boldsymbol{P}_{A2}-\boldsymbol{T}\boldsymbol{P'}_{B2}\right)^{\mathrm{T}}\begin{bmatrix}\frac{\partial\boldsymbol{T}}{\partial z} & \frac{\partial\boldsymbol{T}}{\partial\theta_r} & \frac{\partial\boldsymbol{T}}{\partial\theta_p} & \frac{\partial\boldsymbol{T}}{\partial\theta_y}\end{bmatrix}\boldsymbol{P'}_{B2}\\ \left(\boldsymbol{P}_{A3}-\boldsymbol{T}\boldsymbol{P'}_{B3}\right)^{\mathrm{T}}\begin{bmatrix}\frac{\partial\boldsymbol{T}}{\partial z} & \frac{\partial\boldsymbol{T}}{\partial\theta_r} & \frac{\partial\boldsymbol{T}}{\partial\theta_p} & \frac{\partial\boldsymbol{T}}{\partial\theta_y}\end{bmatrix}\boldsymbol{P'}_{B3}\\ \left(\boldsymbol{P}_{A4}-\boldsymbol{T}\boldsymbol{P'}_{B4}\right)^{\mathrm{T}}\begin{bmatrix}\frac{\partial\boldsymbol{T}}{\partial z} & \frac{\partial\boldsymbol{T}}{\partial\theta_r} & \frac{\partial\boldsymbol{T}}{\partial\theta_p} & \frac{\partial\boldsymbol{T}}{\partial\theta_y}\end{bmatrix}\boldsymbol{P'}_{B4}\end{bmatrix},$$

where diag(·) is a function that expands a vector into a diagonal matrix; $\boldsymbol{e}_3=[0\ 0\ 1]^{\mathrm{T}}$.

3 Training Capability Targeted MPO

Considering that the driving power has limitations, constraint conditions of the MPO model will be established. Then, a training ability evaluation index will be proposed based on inclination angle, critical speed and critical acceleration of the moving platform. By defining the disturbance Lagrange function, another training ability evaluation index will be proposed as a contrast. At last, MPO model of the 4-PSS/PS mechanism will be given.

3.1 Constraint Conditions of the MPO Model

Singularities of parallel mechanisms can be divided into three categories: direct singularity, inverse singularity and combined singularity. The direct singularity makes mechanisms unable to bear loads on the moving platform in singular DOFs, while the inverse singularity leads to movement incapacity of the moving platform in singular DOFs. The combined singularity is the situation when the above two singularities take place simultaneously. Because the direct singularity results in undetermined motions, mechanisms can not work on the direct singular

configurations. Based on definition of the direct singularity, the singularity constraint condition can be written as

$$C_s(\boldsymbol{x}) = |\boldsymbol{B}(\boldsymbol{x})\boldsymbol{B}(\boldsymbol{x}_0)| > 0, \tag{5}$$

where $\boldsymbol{x}_0$ is the initial configuration of the moving platform. Eq. (5) limits that determinants of the matrixes $\boldsymbol{B}$ corresponding to the configurations $\boldsymbol{x}$ and $\boldsymbol{x}_0$ have the same sign, which is equivalent to that the configurations $\boldsymbol{x}$ and $\boldsymbol{x}_0$ are limited in the same nonsingular workspace. This will be revealed in Section 4 by the workspace analysis results.

Considering speed limitation of the active kinematics pairs, the max speed constraint can be given as

$$\boldsymbol{C}_v(\boldsymbol{x}, \dot{\boldsymbol{x}}) = \dot{\boldsymbol{Z}}_{\max} - \mathrm{abs}\left[\boldsymbol{A}^{-1}(\boldsymbol{x})\boldsymbol{B}(\boldsymbol{x})\dot{\boldsymbol{x}}\right] > 0, \tag{6}$$

where abs(·) is the absolute value function, $\dot{\boldsymbol{Z}}_{\max} = \left[\dot{z}_{1\max}\ \dot{z}_{2\max}\ \dot{z}_{3\max}\ \dot{z}_{4\max}\right]^{\mathrm{T}}$ is rated speed vector of the four active prismatic pairs. Here, comparison operations are defined to be elementally conducted.

Considering the driving power limitation, the acceleration constraint can be written as

$$\boldsymbol{C}_a(\boldsymbol{x}, \boldsymbol{a}_p, \boldsymbol{a}_r) = \boldsymbol{F}_{\max}^{\mathrm{T}} - \mathrm{abs}\left[\boldsymbol{Q}^{\mathrm{T}}(\boldsymbol{x}, \boldsymbol{a}_p, \boldsymbol{a}_r)\boldsymbol{B}^{-1}(\boldsymbol{x})\boldsymbol{A}(\boldsymbol{x})\right] > 0, \tag{7}$$

where $\boldsymbol{a}_p$ and $\boldsymbol{a}_r$ are the center-of-mass (COM) acceleration vectors of the moving platform and the robot respectively; $\boldsymbol{F}_{\max} = [F_1, F_2, F_3, F_4]^{\mathrm{T}}$ is rated driving force vector of the active kinematics pairs; $\boldsymbol{Q}$ is the generalized force vector, which is calculated by Eq. (8):

$$\boldsymbol{Q}(\boldsymbol{x}, \boldsymbol{a}_p, \boldsymbol{a}_r) = \begin{bmatrix} \begin{bmatrix} \boldsymbol{e}_r \\ \boldsymbol{e}_p \\ \boldsymbol{e}_y \end{bmatrix} (m_p\boldsymbol{P}_p + m_r\boldsymbol{P}_r) \times (\boldsymbol{g} - \boldsymbol{a}_p - \boldsymbol{a}_r) \\ (m_p + m_r)\boldsymbol{e}_r(\boldsymbol{g} - \boldsymbol{a}_p - \boldsymbol{a}_r) \end{bmatrix}, \tag{8}$$

where m_p and m_r are mass of the moving platform and the robot respectively; $\boldsymbol{P}_p$ and $\boldsymbol{P}_r$ are the COM position vectors of the moving platform and the robot respectively; $\boldsymbol{g}$ is the gravity acceleration vector; $\boldsymbol{e}_r$, $\boldsymbol{e}_p$, $\boldsymbol{e}_y$ are arrays and can be calculated by

$$\begin{cases} \boldsymbol{e}_r = \begin{bmatrix} 0 & 0 & 1 \end{bmatrix}, \\ \boldsymbol{e}_p = \begin{bmatrix} 0 & 1 & 0 \end{bmatrix}\boldsymbol{R}_3^{\mathrm{T}}(\theta_r), \\ \boldsymbol{e}_y = \begin{bmatrix} 1 & 0 & 0 \end{bmatrix}\boldsymbol{R}_2^{\mathrm{T}}(\theta_p)\boldsymbol{R}_3^{\mathrm{T}}(\theta_r), \end{cases}$$

where $\boldsymbol{R}_2(\theta_p)$ and $\boldsymbol{R}_3(\theta_r)$ are rotation matrixes around y axis and z axis with θ_p and θ_r respectively. In order to reduce motor power needed by the training platform, assistant supporting mechanism that bears gravity of the moving platform and the robot is installed on the moving platform. So the fourth element of $\boldsymbol{Q}$ can be changed into 0.

3.2 Stability-training Evaluation Indexes

The valid workspace volume of a mechanism is a general performance evaluation. It can only reflect part of the stability-training ability of the 4-PSS/PS mechanism. So regarding to the training ability of every configuration, two evaluation indexes, which consider the training intensity within the workspace, will be proposed in different aspects here and compared in the next section.

The 4-PSS/PS mechanism simulates disturbances in real environment by random motions. The trained robots adjust their movements to against these disturbances. So the ability of exerting disturbances can evaluate the training ability, which can be calculated in three aspects:

(1) Intensity of the inertial force disturbance on robots' COM, which is formed by the velocity varying motion of the platform. It can be evaluated by average norm of robots' COM critical acceleration and denoted by $n_a(\boldsymbol{x})$.
(2) Lasting time of the mentioned inertial force disturbance. It can be evaluated by average norm of the moving platform's critical velocity and denoted by $n_s(\boldsymbol{x})$.
(3) Inclination disturbance of the moving platform, which can be evaluated by average norm of the moving platform's inclination angle vector and denoted by $n_t(\boldsymbol{x})$.

$n_a(\boldsymbol{x})$, $n_s(\boldsymbol{x})$ are respectively calculated by normalized numerical integration in the robot COM acceleration space and the velocity space of the moving platform. Along with $n_t(\boldsymbol{x})$, they have the following formulae as

$$n_a(\boldsymbol{x}) = \frac{1}{\sqrt{3}N^2}\sum_{i=1}^{N}\sum_{j=1}^{N}\left\|\mathrm{diag}\left(\begin{bmatrix} c_{a1} \\ c_{a2} \\ c_{a3} \end{bmatrix}\right)\boldsymbol{a}_{\max}(\boldsymbol{x}, \alpha_i, \beta_j)\right\|, \tag{9}$$

$$n_s(\boldsymbol{x}) = \frac{1}{\sqrt{4}N^3}\sum_{i=1}^{N}\sum_{j=1}^{N}\sum_{k=1}^{N}\left\|\mathrm{diag}\left(\begin{bmatrix} c_{v1} \\ c_{v2} \\ c_{v3} \\ c_{v4} \end{bmatrix}\right)\dot{\boldsymbol{x}}_{\max}(\boldsymbol{x}, \alpha_i, \beta_j, \gamma_k)\right\|, \tag{10}$$

$$n_{\mathrm{t}}(\boldsymbol{x}) = \frac{1}{\sqrt{2}}\left\|\mathrm{diag}\left(\begin{bmatrix}0 & c_{\mathrm{t1}} & c_{\mathrm{t2}} & 0\end{bmatrix}^{\mathrm{T}}\right)\boldsymbol{x}\right\|, \tag{11}$$

where c_{v1}, c_{v2}, c_{v3}, c_{v4}, c_{a1}, c_{a2}, c_{a3}, c_{t1}, c_{t2} are normalization factors of $\dot{\theta}_{\mathrm{r}}$, $\dot{\theta}_{\mathrm{p}}$, $\dot{\theta}_{\mathrm{y}}$, $\dot{z}$, a_x, a_y, a_z, θ_{p}, θ_{y} respectively. These normalization factors are reciprocals of motion performance requirements to the training platform, which will be given in the next section in details. α_i, β_j, γ_k are super-spherical coordinate variables and $\alpha_i = 2\pi i/N$, $\beta_j = \pi j/N - \pi/2$, $\gamma_k = \pi k/N - \pi/2$ $(i,\ j,\ k = 1,\ 2,\ldots,\ N)$, in which N is the discrete point number. In the direction determined by α_i, β_j in the robot COM acceleration space, $\boldsymbol{a}_{\max}$ is the acceleration vector with the max norm under the acceleration constraint that $\boldsymbol{C}_{\mathrm{a}}(\boldsymbol{x}, \boldsymbol{a}_{\mathrm{p}}, \boldsymbol{a}_{\max}) > 0$. With a variable $r_{\max}$ determined by the dichotomy method, $\boldsymbol{a}_{\max}$ can be written as

$$\boldsymbol{a}_{\max}(\boldsymbol{x}, \alpha_i, \beta_j) = r_{\max}\begin{bmatrix}\cos\alpha_i\cos\beta_j & \sin\alpha_i\cos\beta_j & \sin\beta_j\end{bmatrix}^{\mathrm{T}}. \tag{12}$$

Similarly, $\dot{\boldsymbol{x}}_{\max}$ is the max-normed velocity vector under the speed constraint ($\boldsymbol{C}_{\mathrm{v}}(\boldsymbol{x}, \dot{\boldsymbol{x}}_{\max}) > 0$) in the direction fixed by α_i, β_j, γ_k in platform's velocity space. Also, it is solved by the dichotomy method and has following form of

$$\dot{\boldsymbol{x}}_{\max}(\boldsymbol{x}, \alpha_i, \beta_j, \gamma_k) = r_{\max}\begin{bmatrix}\cos\alpha_i\cos\beta_j\cos\gamma_k \\ \sin\alpha_i\cos\beta_j\cos\gamma_k \\ \sin\beta_j\cos\gamma_k \\ \sin\gamma_k\end{bmatrix}. \tag{13}$$

Because robot balancing movement tends to keep the system dynamics states unchanged or changing slowly, the inertial force of the robot is always declined. As a stricter assumption, the moving platform and the robot can be assumed to be fixed together when solving the $\boldsymbol{a}_{\max}$ by the constraint (7). So $\boldsymbol{a}_{\mathrm{p}}$ can be calculated by

$$\boldsymbol{a}_{\mathrm{p}} = \boldsymbol{a}_{\max} + \dot{\boldsymbol{\omega}} \times (\boldsymbol{P}_{\mathrm{p}} - \boldsymbol{P}_{\mathrm{r}}) + \boldsymbol{\omega} \times [\boldsymbol{\omega} \times (\boldsymbol{P}_{\mathrm{p}} - \boldsymbol{P}_{\mathrm{r}})], \tag{14}$$

where $\boldsymbol{\omega}$ is angle velocity vector of the moving platform, and can be calculated by

$$\boldsymbol{\omega} = \begin{bmatrix}\boldsymbol{e}_{\mathrm{r}}^{\mathrm{T}} & \boldsymbol{e}_{\mathrm{p}}^{\mathrm{T}} & \boldsymbol{e}_{\mathrm{y}}^{\mathrm{T}}\end{bmatrix}\begin{bmatrix}\dot{\theta}_{\mathrm{r}} & \dot{\theta}_{\mathrm{p}} & \dot{\theta}_{\mathrm{y}}\end{bmatrix}^{\mathrm{T}}. \tag{15}$$

Based on Eqs. (9)–(11), we use the following index $I_1(\boldsymbol{x})$ to evaluate the training ability of configuration $\boldsymbol{x}$.

$$I_1(\boldsymbol{x}) = n_{\mathrm{a}}(\boldsymbol{x}) + n_{\mathrm{s}}(\boldsymbol{x}) + n_{\mathrm{t}}(\boldsymbol{x}).$$

By numerical integration in the non-singular workspace, object function E_1 can be given as

$$E_1 = \sum_{\boldsymbol{x}_{\min} \le \boldsymbol{x} \le \boldsymbol{x}_{\max}} I_1(\boldsymbol{x}), \tag{16}$$

where $\boldsymbol{x}_{\min}$ and $\boldsymbol{x}_{\max}$ are the lower bound and the upper bound of $\boldsymbol{x}$ respectively, which limit the maximum workspace in the optimization computation.

Different from the E_1, another object function E_2 is proposed here, which integrates velocity, acceleration and inclination of the moving platform by the disturbance Lagrange function L_{d}. L_{d} is defined as

$$L_{\mathrm{d}} = \frac{1}{2}m_{\mathrm{r}}\boldsymbol{v}_{\mathrm{r}}^{\mathrm{T}}\boldsymbol{v}_{\mathrm{r}} - m_{\mathrm{r}}\|\boldsymbol{g}\|h\cos\alpha, \tag{17}$$

where $\boldsymbol{v}_{\mathrm{r}}$ is velocity of the robot's COM when assuming the robot is fixed with the moving platform, h is the distance between the robot's COM and the moving platform, α is inclination angle of the moving platform. $\boldsymbol{v}_{\mathrm{r}}$ and α can be calculated respectively by

$$\boldsymbol{v}_{\mathrm{r}} = \boldsymbol{\omega} \times \left(\boldsymbol{P}_{\mathrm{r}} - \begin{bmatrix}0 & 0 & z\end{bmatrix}^{\mathrm{T}}\right) + \begin{bmatrix}0 & 0 & \dot{z}\end{bmatrix}^{\mathrm{T}}, \tag{18}$$

$$\alpha = \cos^{-1}(\cos\theta_p\cos\theta_y). \tag{19}$$

Derivative function of L_{d} reflects changing speed of the system dynamic states under disturbances. So the evaluation index $I_2(\boldsymbol{x})$ is defined as

$$I_2(\boldsymbol{x}) = \max(|\mathrm{d}L_{\mathrm{d}}(\boldsymbol{x})/\mathrm{d}t|).$$

And the object function E_2 is defined as

$$E_2 = \sum_{\boldsymbol{x}_{\min} \le \boldsymbol{x} \le \boldsymbol{x}_{\max}} I_2(\boldsymbol{x}). \tag{20}$$

3.3 Mathematical Model of the MPO Problem

Because size of the moving platform can be determined by the trained robots' sizes, L_3 and L_4 among the mechanism parameters can be predetermined. L_0, L_1, L_2 are regarded as the designation variables. Integrating the given constraint conditions and the object functions, the following optimization model can be given as

$$\begin{aligned}&\max_{L_0, L_1, L_2} \quad E, \\ &\text{s.t., } \boldsymbol{x}_{\min} \le \boldsymbol{x} \le \boldsymbol{x}_{\max}, \quad L_{0\min} \le L_0 \le L_{0_{\max}}, \\ &L_{1\min} \le L_1 \le L_{1\max}, \quad L_{2\min} \le L_2 \le L_{2\max}, \\ &C_{\mathrm{s}}(\boldsymbol{x}) > 0, \quad \boldsymbol{C}_{\mathrm{v}}(\boldsymbol{x}, \dot{\boldsymbol{x}}) > 0, \quad \boldsymbol{C}_{\mathrm{a}}(\boldsymbol{x}, \boldsymbol{a}_{\mathrm{p}}, \boldsymbol{a}_{\mathrm{r}}) > 0,\end{aligned} \tag{21}$$

where E can be chosen to be E_1 or E_2; $L_{0\min}$, $L_{1\min}$, $L_{2\min}$, $L_{0\max}$, $L_{1\max}$, $L_{2\max}$ are the minimum values and the maximum values of the designation variables respectively.

4 Case Study Based on the PSO Algorithm

The kinematics calculation, the dynamics calculation and integrations in the workspace involved in the calculation of E_1 and E_2 will lead to strong nonlinearity. So there may be multiple peaks for the proposed object functions. The gradient based algorithms, such as the climbing method and the Lagrange multiplier method, can only converge to the local optimal solutions in this situation. Compared with other global searching algorithms (the genetic algorithm, the simulated annealing algorithm, etc.), the PSO algorithm [33] can speed up the convergence process by using both the "individual experience" and the "global experience". And tuning of the PSO algorithm is much simpler than the model approximation algorithms (artificial neural network, etc.). So the PSO is used here to solve the MPO model.

4.1 Performance Requirement Analysis of the 4-PSS/PS Mechanism Regarding to Stability-training

The 4-PSS/PS mechanism is the parallel mechanism part of the training platform [15, 16], which should has the ability to make the trained robots unstable. So inclination of the moving platform should have the ability to overturn the trained robots in the two horizontal rotation DOFs, and should have a certain motion range in the rest DOFs to provide sufficient room for achieving the speed and acceleration required by the stability training.

Parameters of five legged robots (shown in Table 1) are referenced here to determine the performance requirements for the 4-PSS/PS mechanism. Among them, the GoRoBoT-III is a 70-DOF humanoid robot developed by the authors' laboratory in 2012. It has highly integrated humanoid head, toe joints for humanoid walking, arms and hands for intense gripping. The critical inclination angles are calculated based on parameters of these robots. Calculation results and the robots' parameters are shown in Table 1. The five robots considered here are representative in aspects of mass, size, number and configuration of DOFs, motion capability, so the performance requirements determined for the 4-PSS/PS mechanism are general performance requirements of the stability-training process for legged robots.

Based on the max step length and the robot mass in the Table 1, the minimum size of the moving platform is determined to be 2.5 m × 1.5 m and rated load of the platform is determined to be 110 kg, so that all the robots in Table 1 can be trained on the platform designed and can have a certain moving space (four steps forward walking and 180° turning). Based on the critical overturning angle data in Table 1, required motion range and speed range

Table 1 Parameters and the critical overturning angle of the 5 legged robots

Robot name	DOF number n_{DOF}	Mass m_r (kg)	Height h_r (mm)	Standing support surface size $l_X \times l_Y$ (mm × mm)	Max step length l_S (mm)	The COM height h (mm)	Critical overturning angle in the sagittal plane θ_S (°)	Critical overturning angle in the lateral plane θ_L (°)
HRP-2P [34]	30	54.1	1600	185 × 320*	400	960	5.5	9.5
ASIMO [35]	34	43	1200	220 × 320*	370	720	8.7	12.5
GoRoBoT-III	70	90	1580	200 × 250	380	950	6.0	7.5
TITAN-XIII [36]	12	5.2	300	420 × 420	200	450	25.0	25.0
BigDog [37]	20	109	1000	1100 × 300	300	1500	20	5.7

1. The COM (center of mass) height h of the biped robot is assumed to be 60% of the robot height. Because the quadruped robots are usually loaded weights on their torsos, h of the quadruped robot is assumed to be 150% of the robot height

2. The standing support surface size $l_X \times l_Y$ is measured from the minimum circumscribed rectangle of the robot's support polygon when the robot is in its standing posture

3. Parameters marked by '*' is estimated in proportion of the robot height by the opened image or video data of the robot

4. The max step length l_S of the robot is estimated in proportion of the robot leg length by the opened image or video data of the robot; l_S of the quadruped robot is estimated for the trot gait

Table 2 Required range of the position and orientation variables and their speed

Symbol of the position and orientation parameters	The required range	The required speed range
Roll angle θ_r (°)	[− 15, 15]	[− 5, 5] (°)/s
Pitch angle θ_p (°)	[− 28, 28]	[− 5, 5] (°)/s
Yaw angle θ_y (°)	[− 28, 28]	[− 5, 5] (°)/s
Translation distance z (mm)	[0, 300]	[− 50, 50] mm/s

of the four position and orientation variables of the moving platform are shown in Table 2.

Statistical values of short time accelerations often borne by human are referenced to determine the acceleration requirements of the moving platform. For examples, acceleration of an airplane takeoff is about 0.5*g* (gravity acceleration value of the earth); elevator's maximum acceleration of normal working is about 0.3*g*; sudden braking acceleration of a bus running at 112.7 km/h is approximately 0.4*g* [38]. So the critical acceleration value of human to lose stability is assumed to be 0.4*g*, which can also be used as the maximum acceleration value required for the stability training. In the continuous working statue, the motion platform is required to make the robot's COM to achieve the 0.4*g* acceleration in any direction. Also, capability of short time overloading is required for some disturbance with larger acceleration but shorter acting time, so that the platform can simulate the real environments.

4.2 Optimization Calculation for the 4-PSS/PS Mechanism Using the PSO Algorithm

Optimization program is coded in the Matlab software and is run in a personal computer with the 2.99 GHz Pentium Dual-Core E5700 CPU. For the 4-PSS/PS parallel mechanism, particles of the PSO algorithm are defined to be: $\boldsymbol{p}_i = [L_{0,i}, L_{1,i}, L_{2,i}]^{\mathrm{T}}$ (i is an index of particles). After multiple tunings, the particle number is chosen to be 15, which makes the algorithm prefer to get the global optimal solution within reasonable time consumption. And in order to enhance the ability of jumping out from local solutions, bigger study ratio and inertial factor are used, which are respectively set to be 1 and 0.85. The PSO algorithm will be terminated after the iteration number n_{I} achieving the max tolerant, which is set to be 400 (determined by multiple tunings). For the moving platform of 2500 mm × 1500 mm, values of other parameters involved in the optimization calculation are shown in Table 3.

Choosing the object function to be E_1 and E_2 separately, the MPO model is solved plenty times. They all get the same optimal solution before n_{I} achieving the max tolerant, among which E_1 and E_2 curves of three solving processes are shown in Figure 3(a) and Figure 3(b) respectively.

The PSO algorithm is convergent in $[2500.0000, 1954.6664, 1000.0000]^{\mathrm{T}}$ mm and $[2500.0000, 2040.2948, 1000.0000]^{\mathrm{T}}$ mm respectively for E_1 and E_2 under the residuals tolerance of 10^{-4} mm. They are rounded into $[2500, 1955, 1000]^{\mathrm{T}}$ mm and $[2500, 2040, 1000]^{\mathrm{T}}$ mm respectively for actual mechanism designation. The maximum values of the E_1 and E_2 are 5.9352×10^7 and 20.104 kW respectively. The calculation times are 4.5 h and 11.8 h, respectively.

4.3 Workspace Analysis for the Optimization Results

The workspaces corresponding to the two mechanism parameter sets are analyzed here. Boundaries of theoretical workspace are solved for the 4-PSS/PS mechanism based on its kinematics model. Also, critical surfaces are solved for the singularity constraint, the max speed constraint and the acceleration constraint. Then the

Table 3 Parameter values involved in the optimization calculation

Parameter	Value
Maximum boundary of designation variables $[L_{0\max}, L_{1\max}, L_{2\max}]$ (mm)	[1000, 3500, 2500]
Minimum boundary of designation variables $[L_{0\min}, L_{1\min}, L_{2\min}]$ (mm)	[400, 2500, 1500]
Rotation speed's normalization factors $[c_{\mathrm{v}1}, c_{\mathrm{v}2}, c_{\mathrm{v}3}]$ (s/rad)	[11.46, 11.46, 11.46]
Translation speed's normalization factors $c_{\mathrm{v}4}$ (s/mm)	0.02
Acceleration's normalization factors $[c_{\mathrm{a}1}, c_{\mathrm{a}2}, c_{\mathrm{a}3}]$ (s^2/m)	[0.2251, 0.2251, 0.2251]
Moving range's normalization factors $[c_{\mathrm{t}1}, c_{\mathrm{t}2}]$ (/rad)	[2.046, 2.046]
Moving platform's size $L_3 \times L_4$ (m × m)	2.5 × 1.5
Height of the robot's COM h (mm)	700
Robot's mass m_{r} (kg)	90
Moving platform's mass m_{p} (kg)	20
Active pairs' max speed $\dot{\boldsymbol{Z}}_{\max}$ (mm/s)	$[250, 250, 250, 250]^{\mathrm{T}}$
Max driving force $\boldsymbol{F}_{\max}$ (N)	$[1450, 1450, 1450, 1450]^{\mathrm{T}}$
Upper boundary of platform's rotation angle $[\theta_{\mathrm{rmax}}, \theta_{\mathrm{pmax}}, \theta_{\mathrm{ymax}}]$ (°)	[15, 29]
Lower boundary of platform's rotation angle $[\theta_{\mathrm{rmin}}, \theta_{\mathrm{pmin}}, \theta_{\mathrm{ymin}}]$ (°)	[− 15, − 28, − 28]
Upper boundary of platform's translation distance $z_{\max}$ (mm)	300
Lower boundary of platform's translation distance $z_{\min}$ (mm)	0
Discrete point number N	30
Gravity acceleration vector $\boldsymbol{g}$ ($\mathrm{m/s}^2$)	$[0, 0, -9.8]^{\mathrm{T}}$

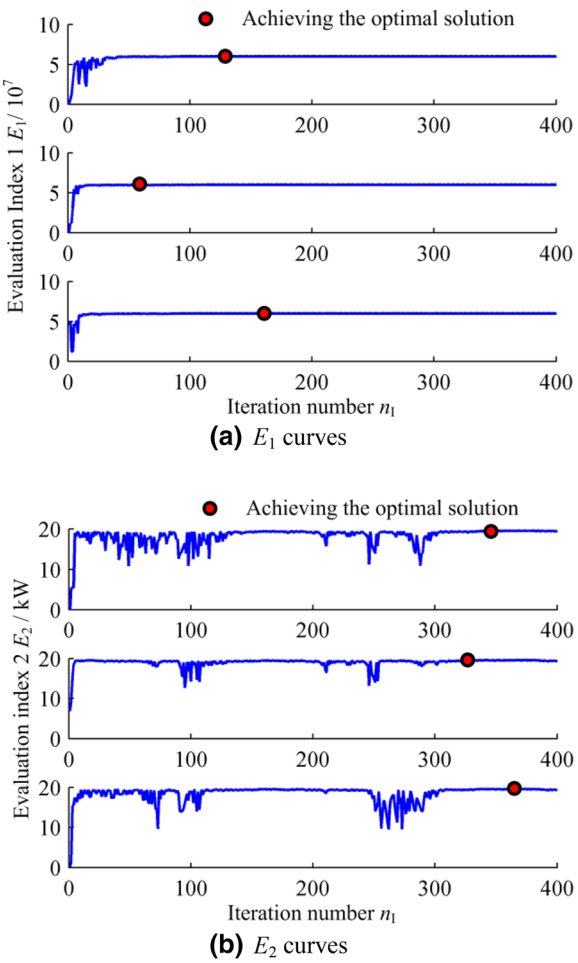

Figure 3 E_1 and E_2 curves of three solving processes

theoretical workspace boundary and the critical surfaces in it are integrated to get the valid workspace boundaries corresponding to the two mechanism parameter sets. The mechanism parameter set with larger valid workspace is regarded as the final optimal result.

To display the 4-dimensional workspace of the 4-PSS/PS mechanism, z value among the position and orientation parameters is fixed, so the subspaces spanned by the rest three orientation angles can be displayed in the Cartesian coordinate frame. The whole workspace is displayed by splicing these subspaces with different z values. Because the axis directions of the four active prismatic pairs are parallel with the moving direction of the z axis translation DOF, the subspaces with different z value will be exactly the same with unlimited movement range of the active prismatic pairs. In different subspaces, the differences of the corresponding joint variables will be equal to the difference of the z values. Thus the whole 4-dimensional workspace of the 4-PSS/PS mechanism can be displayed by the 3-dimensional orientation angle space without loss of generality when z is set to 0. The process of solving the valid workspace is shown in Figure 4.

In Figure 4, the theoretical workspace boundary surface and the critical surfaces need to be calculated first. Then the valid workspace boundary surface of the 4-PSS/PS mechanism is the inner envelope surface of these surfaces. The initial configuration is chosen to be $\boldsymbol{x}_0 = [0\ 0\ 0\ 0]^{\mathrm{T}}$, and the dichotomy method is used solve intersection points between the above mentioned surfaces and a straight line from the $\boldsymbol{x}_0$. Among them, the theoretical workspace boundary is identified by whether or not inverse kinematics (IK) of the mechanism has real solutions. In each line from $\boldsymbol{x}_0$, the boundary point of the valid workspace is the nearest point to $\boldsymbol{x}_0$ among the theoretical boundary point and critical point of constraint conditions. The boundary surface of the valid workspace can be obtained by swapping the workspace.

$\boldsymbol{V}$ and $\boldsymbol{A}$ are velocity space of the moving platform and acceleration space of the robot's COM respectively. Values of $\boldsymbol{V}$ and $\boldsymbol{A}$ can be determined by the performance requirements of the 4-PSS/PS mechanism, and are shown as

$$\boldsymbol{V} = \left\{ \dot{\boldsymbol{x}} = \left[\dot{\theta}_{\mathrm{r}}\ \dot{\theta}_{\mathrm{p}}\ \dot{\theta}_{\mathrm{y}}\ \dot{\boldsymbol{z}} \right]^{\mathrm{T}} \middle| \begin{array}{l} -5(^\circ)/\mathrm{s} \le \dot{\theta}_{\mathrm{r}}, \dot{\theta}_{\mathrm{p}}, \dot{\theta}_{\mathrm{y}} \le 5(^\circ)/\mathrm{s}, \\ -50\ \mathrm{mm/s} \le z \le 50\ \mathrm{mm/s} \end{array} \right\}.$$

$$\boldsymbol{A} = \{\boldsymbol{a} \in \boldsymbol{R}^3 | (\boldsymbol{a} (\le 0.4g\}.$$

Figure 5 shows the workspace analysis results when the mechanism parameters with unit of mm are $L_0 = 1000$, $L_1 = 2500$, $L_2 = 1955$, $L_3 = 2500$, $L_4 = 1500$ (optimization result for E_1) and $L_0 = 1000$, $L_1 = 2500$, $L_2 = 2040$, $L_3 = 2500$, $L_4 = 1500$ (optimization result for E_2) respectively. The workspace analysis is conducted in the same personal computer with the MPO calculation. The computational time is nearly 1.5 h for each parameter set.

The boundary surfaces and the critical surfaces of the constraint conditions shown in Figure 5 are surfaces central symmetry with respect to the origin point. It is also shown that the theoretical workspace of the 4-PSS/PS mechanism is segmented into three subspaces by the singular surfaces. Determinant of the matrix $\boldsymbol{B}(\boldsymbol{x})$ keeps the same sign in each subspace and changes its sign when $\boldsymbol{x}$ crosses the singular surfaces. So the singularity constraint condition given in Section 2 by Eq. (5) is equal to

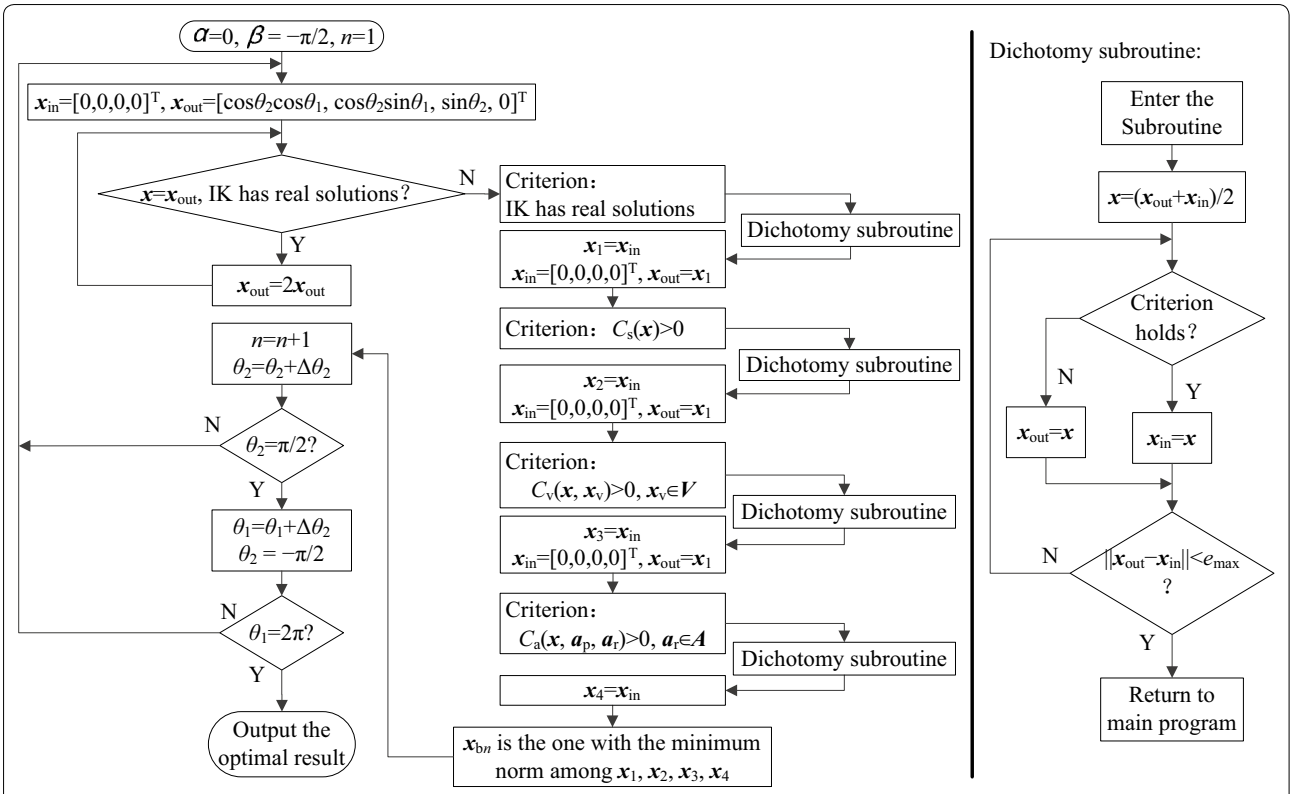

Figure 4 Process of the valid workspace boundary extracting algorithm

that configuration $\boldsymbol{x}$ is in the same nonsingular subspace with $\boldsymbol{x}_0$. By integrating the surfaces in Figure 5, boundary surfaces of the valid workspaces corresponding to the MPO results of E_1 and E_2 are obtained and are shown in Figure 6.

In order to give a clear view, $\theta_y > 0$ parts of the valid workspace boundaries are hidden in Figure 6. In these valid workspaces, moving range of the platform can reach: $-29.7° \le \theta_r \le 29.7°$, $-31.5° \le \theta_p \le 31.5°$, $-56.7° \le \theta_y \le 56.7°$. This moving range is bigger than the required moving range of the moving platform shown in Table 2. So, after the MPO process, the designed training platform can be used to train all the legged robots shown in Table 1. It is also revealed that differences between those two valid workspaces are quit small and the optimization result of the object function E_2 is better than the one of E_1 in aspect of the valid workspace volume. So the final optimal mechanism parameters are chosen to be $L_0 = 1000$ mm, $L_1 = 2500$ mm, $L_2 = 2040$ mm, $L_3 = 2500$ mm, $L_4 = 1500$ mm.

But the computational time cost of the object function E_2 is much higher than E_1. So in a MPO with a higher dimensional parameter set (when moving platform size is not determined or the serial DOF is also considered in the MPO process), E_1 can be used as an approximation of E_2.

5 Conclusions

(1) Two object functions are proposed using the normalized motion indexes and the disturbance Lagrange function respectively. Both of these object functions consider the training ability evaluation and the workspace size simultaneously, which solves the existing MPO methods' problem of only focusing on the singularity issue or workspace size of parallel mechanisms.

(2) The MPO model is solved by the PSO algorithm. It is revealed that the valid workspace corresponding to each evaluation's result is quite similar. So the two proposed evaluations can reflect the stability-training ability of the platform consistently.

(3) Based on the proposed constraint conditions (the singularity constraint, the max speed constraint, the acceleration constraint), the valid workspaces of the MPO results are analyzed. Moving range of the platform can reach: $-29.7° \le \theta_r \le 29.7°$, $-31.5° \le \theta_p \le 31.5°$, $-56.7° \le \theta_y \le 56.7°$. This moving range satisfies training requirement of the five typical legged robots. Also, the proposed three

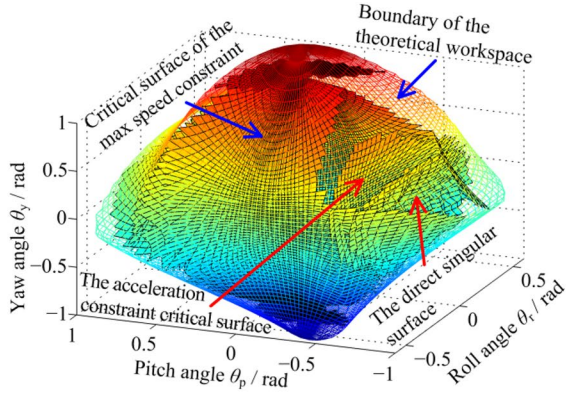

(a) Workspace of the 4-PSS/PS mechanism when L_0=1000 mm, L_1=2500 mm, L_2=1955 mm, L_3=2500 mm, L_4=1500 mm

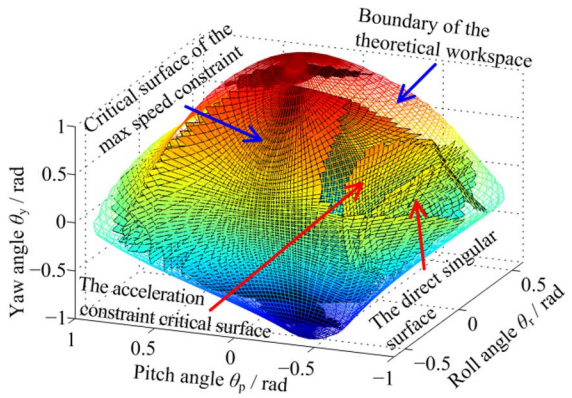

(b) Workspace of the 4-PSS/PS mechanism when L_0=1000 mm, L_1=2500 mm, L_2=2040 mm, L_3=2500 mm, L_4=1500 mm

Figure 5 Workspace of the 4-PSS/PS mechanism for the two optimization results

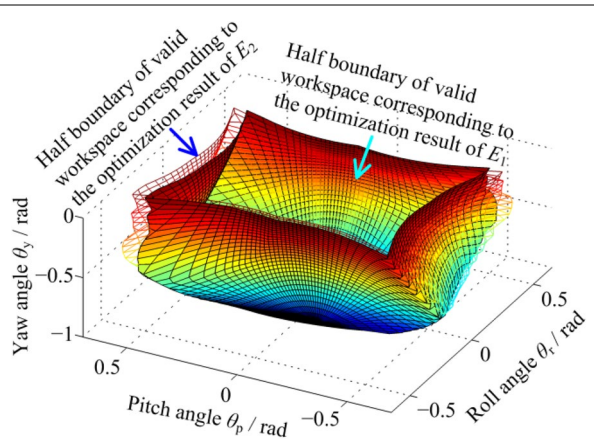

Figure 6 Valid workspace boundary of the 4-PSS/PS mechanism corresponding to the two optimal mechanism parameter sets

constraint conditions will be used to control the designed training platform by determining safety boundaries of its actual workspace.

Authors' Contributions

W-GW in charge of the whole of theory and analyses. L-YG wrote Sections 3, 4.2 and 4.3 of the manuscript. W-GW wrote Sections 1, 2, 4.1, 5, and modified the manuscript. L-YG assisted with programming and computing. Both authors read and approved the final manuscript.

Authors' Information

Wei-Guo Wu, born in 1966, is currently a professor and PhD tutor at *School of Mechatronics Engineering*, *Harbin Institute of Technology*, *China*. He received his BS degree from *Liaoning Technical University*, *China*, in 1988. Then he received his MS and PhD degree from *Harbin Institute of Technology*, *China*, respectively in 1991 and 1995. From 1999 to 2001, he was a postdoctoral fellow in Nagoya University, Japan. His research interests include: gorilla robot with multiple moving modes and its intelligent motion control, artificial emotion and humanoid robot with expressions and multiple perception functions, industrial robots and basic components of robots, bionic mechanism and mechanics.

Li-Yang Gao, born in 1990, is currently a PhD candidate at *School of Mechatronics Engineering*, *Harbin Institute of Technology*, *China*. He received his BS degree from *Harbin Institute of Technology*, *China*, in 2013. His research interests include: parallel mechanism, intelligent stabilizing control of biped robot.

Competing Interests

The authors declare that they have no competing interests.

Publisher's Note

Received: 27 July 2016 Accepted: 13 June 2018
Published online: 25 June 2018

References

[1] S Kajita, M Morisawa, K Harada, et al. Biped walking pattern generator allowing auxiliary ZMP control. *Int. Conf. on Intelligent Robots and Systems*, Beijing, China: IEEE Press, 2006: 2993–2999.

[2] S Keehong, K Joohyung, R Kyungshik. Towards natural bipedal walking: virtual gravity compensation and capture point control. *International Conference on Intelligent Robots and Systems*, Vilamoura, Algarve, Portugal: IEEE Press, 2012: 4019–4026.

[3] N Kaewlek, T Maneewarn. Inclined plane walking compensation for a humanoid robot. *International Conference on Control, Automation and Systems*, 27–30 Oct. 2010, Gyeonggi-do, Korea: IEEE Press, 2010: 1403–1407.

[4] Y D Kim, I W Park, J K Yoo, et al. Stabilization control for humanoid robot to walk on inclined plane. *8th IEEE-RAS International Conference on Humanoid Robots*, 1–3 Dec. 2008, Daejeon, Korea: IEEE Press, 2008: 28–33.

[5] H Hauser, G Neumann, A J Ijspeert, et al. Biologically inspired kinematic synergies provide a new paradigm for balance control of humanoid robots. *7th IEEE-RAS International Conference on Humanoid Robots* (*HUMANOIDS*), 29 Nov.–1 Dec. 2007, Pittsburgh, USA: IEEE Press, 2007: 73–80.

[6] M Shahbazi, G A D Lopes, R Babuska. Observer-based postural balance control for humanoid robots. *IEEE International Conference on Robotics and Biomimetics* (*ROBIO*), 12–14 Dec. 2013, Shenzhen, China: IEEE Press, 2013: 891–896.

[7] Z Li, N G Tsagarakis, D G Caldwell. Stabilizing humanoids on slopes using terrain inclination estimation. *2013 IEEE/RSJ International Conference on Intelligent Robots and Systems* (*IROS*), 3–7 Nov. 2013, Tokyo, Japan: IEEE Press, 2013: 4124–4129.

[8] Y Yoshida, K Takeuchi, D Sato, et al. Balance control of humanoid robots in response to disturbances in the frontal plane. *Proceedings of the 2011 IEEE International Conference on Robotics and Biomimetics*, 7–11 Dec. 2011, Phuket, Thailand: IEEE Press, 2011: 2241–2242.
[9] C J Zhou, Q C Meng, Dynamic balance of a biped robot using fuzzy reinforcement learning agents. *Fuzzy Sets and Systems*, 2003, 134(1): 169–187.
[10] J P Ferreira, M M Crisostomo, A P Coimbra. SVR versus neural-fuzzy network controllers for the sagittal balance of a biped robot. *IEEE Transactions on Neural Networks*, 2009, 20(12): 1885–1897.
[11] P Hénaff, V Scesa, F B Ouezdou, et al. Real time implementation of CTRNN and BPTT algorithm to learn on-line biped robot balance: Experiments on the standing posture. *Control Engineering Practice*, 2011, 19(1): 89–99.
[12] K S Hwang, J S Li, W C Jiang, et al. Gait balance of biped robot based on reinforcement learning. *2013 Proceedings of SICE Annual Conference* (*SICE*), 14–17 Sept. 2013, Nagoya, Japan: IEEE Press, 2013: 435–439.
[13] R Vuga, M Ogrinc, A Gams, et al. Motion capture and reinforcement learning of dynamically stable humanoid movement primitives. *2013 IEEE International Conference on Robotics and Automation* (*ICRA*), 6–10 May 2013, Karlsruhe, Germany: IEEE Press, 2013: 5284–5290.
[14] M Wasielica. In-motion balance recovery of a humanoid robot under severe external disturbances. In: R Szewczyk, C Zieliński, M Kaliczyńska (eds). *Progress in Automation, Robotics and Measuring Techniques. Advances in Intelligent Systems and Computing*. Springer, 2015, 351: 299–308.
[15] Wei-Guo Wu, Wen-Qian Du. Research of 6DOF serial-parallel mechanism platform for stability training of legged-walking robot. *Journal of Harbin Institute of Technology (New Seriers)*, 2014, 21(2): 75–82.
[16] Wei-Guo Wu, Wen-Qian Du. Six-degree-of-freedom serial-parallel mechanism platform for stability training of legged robots. China, ZL201310250326.5, 2013-10-09[2018-6-17]. (**in Chinese**)
[17] S A A Moosavian, A A Nazari, A Hasani. Kinematics and workspace analysis of a novel 3-DOF spatial parallel robot. *19th Iranian Conference on Electrical Engineering* (*ICEE*), 17–19 May 2011, Tehran, Iran: IEEE Press, 2011: 1–6.
[18] A Wolf, D Glozman. Singularity analysis of large workspace 3RRRS parallel mechanism using line geometry and linear complex approximation. *Journal of Mechanisms and Robotics*, 2011, 3(1): 011004.
[19] H J Liu, S Zhao, S Li, et al. A novel flexible assistant parallel mechanism and dynamic analyses. *2010 IEEE International Conference on Information and Automation (ICIA)*, 20–23 June 2010, Harbin, China: IEEE Press, 2010: 861–866.
[20] H Azulay, M Mahmoodi, R Zhao, et al. Comparative analysis of a new 3×PPRS parallel kinematic mechanism. *Robotics and Computer-Integrated Manufacturing*, 2014, 30(4): 369–378.
[21] T Yoshikawa. Manipulability of Robotic Mechanisms. *The International Journal of Robotics Research*. 1985, 4(2): 3–9.
[22] J Salisbury, J Craig. Articulated hands: Force control and kinematic issues. *The International Journal of Robotics Research*, 1982, 1: 4–17.
[23] C Gosselin, J Angeles. A global performance index for the kinematic optimization of robotic manipulators. *ASME Journal of Mechanical Design*, 1991, 113: 220–226.
[24] S Caro, N Binaud, P Wenger. Sensitivity analysis of 3-RPR planar parallel manipulators. *J. Mech. Des*., 2009, 131(12): 121005.
[25] N Binaud, S Caro, P Wenger. Sensitivity comparison of planar parallel manipulators. *Mech. Mach. Theory*, 2010, 45(11): 1477–1490.
[26] A Rezaei, A Akbarzadeh. Study on Jacobian, singularity and kinematics sensitivity of the FUM 3-PSP parallel manipulator. *Mechanism and Machine Theory*, 2015, 86: 211–234.
[27] M Tannous, S Caro, A Goldsztejn. Sensitivity analysis of parallel manipulators using an interval linearization method. *Mechanism and Machine Theory*, 2014, 71: 93–114.
[28] H Li, C Gosselin, M Richard. Determination of maximal singularity-free zones in the workspace of planar three-degree-of-freedom parallel mechanisms. *Mech. Mach. Theory*, 2006, 41(10): 1157–1167.
[29] J Fu, F Gao, J Chin. Optimal design of a 3-leg 6-DOF parallel manipulator for a specific workspace. *Chinese Journal of Mechanical Engineering*, 2016, 29(4): 659–668.
[30] A Karimi, M T Masouleh, P Cardou. Singularity-free workspace analysis of general 6-UPS parallel mechanisms via convex optimization. *Mechanism and Machine Theory*, 2014, 80: 17–34.
[31] M H F Kaloorazi, M T Masouleh, S Caro. Determination of the maximal singularity-free workspace of 3-DOF parallel mechanisms with a constructive geometric approach. *Mechanism and Machine Theory*, 2015, 84: 25–36.
[32] Y Hou, X Hu, D Zeng, et al. Biomimetic shoulder complex based on 3-PSS/S spherical parallel mechanism. *Chinese Journal of Mechanical Engineering*, 2015, 28(1): 29–37.
[33] J Kennedy, R Eberhart. Particle swarm optimization. *Proceedings of IEEE International Conference on Neural Networks IV*, 1995: 1942–1948. https://doi.org/10.1109/icnn.1995.488968.
[34] H Hirukawa, F Kanehiro, K Kaneko, et al. Humanoid robotics platforms developed in HRP. *Robotics and Autonomous Systems*, 2004, 48(4): 165–175.
[35] H Masato, O Kenichi. Honda humanoid robots development. *Philosophical Transactions of the Royal Society A-Mathematical Physical and Engineering Sciences*, 2007, 365(1850): 11–19.
[36] S Kitano, S Hirose, G Endo, et al. Development of lightweight sprawling-type quadruped robot TITAN-XIII and its dynamic walking. *Intelligent Robots and Systems* (IROS), 3–7 Nov. 2013, Tokyo, Japan: IEEE Press, 2013: 6025–6030.
[37] M Raibert, K Blankespoor, G Nelson, et al. BigDog, the rough-terrain quadruped robot. *IFAC Proceedings Volumes*, 2008, 41(2): 10822–10825.
[38] C M Hams, C E Crede. Shock and vibration handbook. New York: McGraw-Hill, 1976.